ChemComm

COMMUNICATION

View Article Online
View Journal | View Issue

Cite this: *Chem. Commun.*, 2021, 57, 655

Received 10th November 2020,
Accepted 3rd December 2020

DOI: 10.1039/d0cc07398a

rsc.li/chemcomm

An ESIPT-induced NIR fluorescent probe to visualize mitochondrial sulfur dioxide during oxidative stress *in vivo*†

Haixian Ren,[ab] Fangjun Huo,[c] Xia Wu,[d] Xiaogang Liu*[d] and Caixia Yin*[a]

Based on the change in electron distribution of the benzopyrylium unit before and after sulfite addition, a 2-(2′-hydroxyphenyl)benzothiazole (HBT)-based fluorophore generated the excited state intramolecular proton transfer (ESIPT) process with a near-infrared enhanced emission at 836 nm and a large Stokes shift (286 nm). The probe was applied to image SO_2 derivatives in cells and mice. Our data will provide new ideas for the development of ESIPT-based fluorescence probe with longer wavelength emission.

An appropriate balance between oxidants and antioxidants is necessary for the survival of mammalian cells. An imbalance of redox homeostasis can cause metabolic syndrome, DNA damage, and even cancer.[1] Reactive oxygen species (ROS) are the signaling molecules for oxidative stress.[2] Cells can inhibit oxidative stress through endogenous antioxidants under an immune mechanism. Sulfur dioxide (SO_2) is an antioxidant. It can play an important part in maintaining redox homeostasis. SO_2 can be generated in mitochondria with sulfur-containing amino acids (RSS) oxidized by ROS.[3] However, some studies have claimed that SO_2 has oxidative capability in complex biological environments. Thus, the role of SO_2 under oxidative stress must be reassessed.[4] Mitochondria are the main sites of oxidation and phosphorylation. Excess oxidative stress can cause mitochondrial dysfunction. Therefore, exploring the level of SO_2 in mitochondria under oxidative stress will help to further understand the role of SO_2 in maintaining redox homeostasis.

Fluorescent probes are important tools for understanding the biological functions and mechanism of action of important biomolecules.[5] Much effort has been devoted to developing fluorescent probes that target mitochondrial SO_2.[6] We synthesized a series of probes based on the benzopyrylium group, which has a multifunctional unit[7] with a built-in site for sulfite, one positive charge required for targeting mitochondria, and good solubility in water. These probes could detect sulfite with high sensitivity and rapidly, but along with a serious blue shift in the emission spectrum due to the destroyed conjugated system. That feature limited their practical applications in bioimaging because of interference from increased biological autofluorescence. Similar situations have been documented in most other probes that used "C=C" bonds as reaction sites for sulfite (Table S1, ESI†). Near-infrared (NIR) fluorescence imaging could be used due to the decreased autofluorescence background, deep penetration into tissue, and low light scattering.[8] The induced enhanced emission was <700 nm for the reported SO_2 probes,[9] which made them unsuitable for high-precision imaging. Hence, we transferred our interest to building an off–on long-wavelength NIR fluorescent probe for sulfite.

We considered the change in electron density of the benzopyrylium unit before and after sulfite addition, and the special conditions for a 2-(2′-hydroxyphenyl)benzothiazole (HBT)-based fluorophore to generate the excited state intramolecular proton transfer (ESIPT) process. An activated **NIR-TS** probe based on the ESIPT off–on process was designed under the guidance of hole–electron analyses based on time-dependent density-functional theory (TDDFT) calculations. As a response to SO_2, the **NIR-TS** probe was expected to generate NIR enhanced emission with a large Stokes shift, which was an improved signal quantification[10] due to avoidance of autofluorescence inference and detrimental crosstalk[11] between excited and emitted light. The **NIR-TS** probe was synthesized, and characterized by ^{1}H nuclear magnetic resonance (NMR) and ^{13}C NMR spectroscopy and high-resolution mass spectrometry (Scheme S1 and Fig. S1, ESI†). Initially, the spectral response of

[a] *Key Laboratory of Chemical Biology and Molecular Engineering of Ministry of Education, Key Laboratory of Materials for Energy Conversion and Storage of Shanxi Province, Institute of Molecular Science, Shanxi University, Taiyuan 030006, China. E-mail: yincx@sxu.edu.cn*
[b] *Xinzhou Teachers University, Xinzhou 030004, China*
[c] *Research Institute of Applied Chemistry, Shanxi University, Taiyuan 030006, China*
[d] *Singapore University of Technology and Design, 8 Somapah Road, 487372, Singapore*

† Electronic supplementary information (ESI) available. See DOI: 10.1039/d0cc07398a

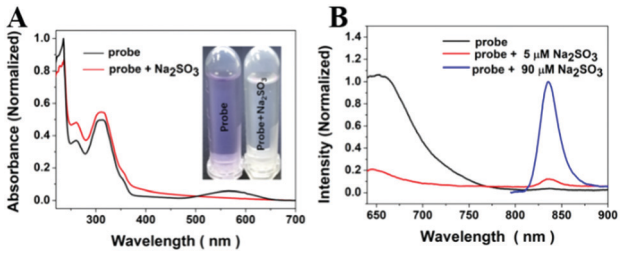

Fig. 1 Spectroscopic responses of the **NIR-TS** probe to Na_2SO_3. (A) Responses of UV-vis absorption spectroscopy of the **NIR-TS** probe (30 μM) towards Na_2SO_3 (100 μM); (B) fluorescent responses of the **NIR-TS** probe (10 μM) towards Na_2SO_3 (5 μM and 90 μM).

the **NIR-TS** probe to SO_2 was investigated using sodium sulfite (Na_2SO_3) as the supply source of SO_2. Absorption of the **NIR-TS** probe peaked at 313 nm and 568 nm, which was attributed to 2-(benzothiazole-2-yl)-4-methylphenol and benzopyrylium groups, respectively. In turn, the **NIR-TS** probe showed emission at 653 nm when excited by 550 nm light (Fig. 1). The red-light emission enabled visualization of mitochondria targeted by the **NIR-TS** probe. After addition of Na_2SO_3 to the **NIR-TS** probe, its absorption at 568 nm decreased with a change from purple to colorless, and the 836 nm emission in the NIR region emerged and increased simultaneously (Fig. 1). The emission reached a plateau upon addition of Na_2SO_3 (90 μM) to the **NIR-TS** probe. Furthermore, a good linear relationship between the emission intensity and Na_2SO_3 concentration was found at 0.5–40 μM (Fig. S2C, ESI†). The limit of detection (LoD) was calculated to be 0.067 μM by the general $3\sigma/k$ method. Some reports have documented sulfite levels of 0–10 μM in the serum of healthy people, and (0–4 μM) in mitochondria.[12] Hence, the **NIR-TS** probe was suitable for sensitive monitoring of Na_2SO_3 levels in a biological system.

The **NIR-TS** probe had excellent photostability at pH 5–10 and had a relatively strong response to Na_2SO_3 at pH 8.0 (Fig. S2D, ESI†). The pH in mitochondria is ~8, so the **NIR-TS** probe could detect SO_2 (and its derivatives) in mitochondria effectively. We also studied the time-dependent spectral response of the **NIR-TS** probe towards Na_2SO_3 (Fig. S3, ESI†). The fluorescent signal at 836 nm leveled off within 10 s, and reached 30-times that of the **NIR-TS** probe itself. This ultrafast and sensitive manner enabled the **NIR-TS** probe to monitor the levels of SO_2 (and its derivatives) in cells.

Subsequently, the selectivity of the **NIR-TS** probe towards Na_2SO_3 was evaluated by treatment with various biologically relevant species: sulfur-containing species, reducing agents, ROS, and other inorganic salts (Fig. S4, ESI†). The changes in fluorescence intensity caused by these competing species were negligible. Hence, the **NIR-TS** probe could monitor levels of SO_2 (and its derivatives) selectively in a complex physiological condition. To confirm further the reaction mechanism of the **NIR-TS** probe towards Na_2SO_3, mass spectrometry was conducted (Fig. S5, ESI†). Addition of Na_2SO_3 to a solution of **NIR-TS** revealed a prominent peak of $[M - H]^-$ at m/z 587.1684, which corresponded to the adduct for **NIR-TS** towards Na_2SO_3 (calcd: 587.1680).

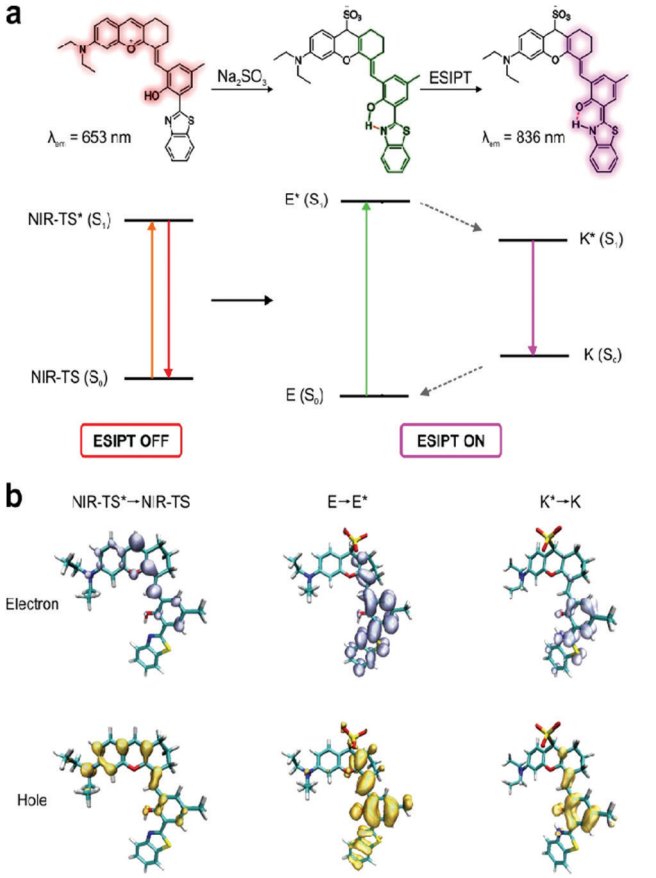

Scheme 1 (a) Design of the **NIR-TS** probe for subcellular SO_2 detection. (b) Calculated electron–hole distributions during photoexcitation of the **NIR-TS** probe in water before and after reactions with SO_2. The geometry of **NIR-TS** and **K** is based on excited-state optimized structures, whereas that of **E** is based on the ground-state optimized structure.

We also conducted quantum chemical calculations to rationalize the spectroscopic properties of **NIR-TS**. Before the reaction with SO_2, the first excited state of **NIR-TS** was dominated by the benzopyrylium moiety with red emissions (highlighted in red; Scheme 1a). This denoted the distribution of the corresponding electrons and holes residing in the benzopyrylium fragment (Scheme 1b and Fig. S6, ESI†). However, upon the reaction with SO_2, the π-conjugation of the benzopyrylium moiety was broken, along with a blue shift in the UV-vis absorption spectrum. Consequently, the distribution of electrons and holes of the first excited state of the newly formed adduct (**E**) shifted to the hydroxybenzothiazole and neighboring unit (highlighted in green; Scheme 1), thereby activating ESIPT. Indeed, further calculations showed that ESIPT was energetically favorable for adduct **E**, and ESIPT led to significantly red-shifted emissions from the ketone form **K** (Scheme 1 and Fig. S6, ESI†).

To explore the capabilities of the **NIR-TS** probe to image SO_2 (Na_2SO_3) in mitochondria, a cytotoxic assay of the **NIR-TS** probe was undertaken in HeLa cells (Fig. S7, ESI†). We discovered that >85% of cells were alive upon treatment with the **NIR-TS** probe (5 μM) for 10 h, which indicated the low cytotoxicity of the

NIR-TS probe. Similar to other mitochondria-targetable probes with positive charges, enrichment of the **NIR-TS** probe in mitochondria was possible.[13] To examine this possibility, colocalization experiments were carried out (Fig. S8, ESI†). Cells treated with the **NIR-TS** probe and the MitoTracker™ Green (mitochondrial stain) exhibited strong emissions in red and green channels. The merged image (Fig. S8c and f, ESI†) indicated that both channels overlaid very well. Pearson's colocalization coefficient was calculated to be 0.82, demonstrating that the **NIR-TS** probe could accumulate specifically in the mitochondria of living cells.

Next, the ability of the **NIR-TS** probe to image Na_2SO_3 in living cells was evaluated (Fig. S9, ESI†). For control cells incubated only with the **NIR-TS** probe, no fluorescence signals were captured in the NIR channel. For cells incubated sequentially with the **NIR-TS** probe and Na_2SO_3, concentration-dependent fluorescence signals were noted in the NIR channel. Hence, the **NIR-TS** probe could detect exogenous Na_2SO_3 with excellent sensitivity in living cells. $Na_2S_2O_3$ can be combined with glutathione *via* thiosulfate sulfurtransferase (TST) to produce endogenous SO_2 derivatives in mammals.[14] To evaluate the ability of the **NIR-TS** probe to detect endogenous SO_2 derivatives, HeLa cells were imaged after treatment with **NIR-TS** and $Na_2S_2O_3$ (500 μM) (Fig. 2c). NIR fluorescence signals were activated due to the GSH-induced generation of SO_2. For confirmation, control cells were prepared by successive treatment of *N*-ethylmaleimide (NEM; thiol inhibitor), the **NIR-TS** probe and $Na_2S_2O_3$ for imaging. Control cells did not produce an obvious NIR fluorescence signal (Fig. 2d). Hence, the **NIR-TS** probe could work as an endogenous SO_2 sensor. Furthermore, lipopolysaccharide (LPS) can also produce low-level sulfite endogenously by inducing an inflammatory response in cells.[15] NIR signals were observed when the **NIR-TS** probe was used to image HeLa cells pretreated with LPS (1 μg mL^{-1}) (Fig. 2e). However, the signals were lost for cells treated with LPS and formaldehyde (FA) due to the inhibition of sulfite by FA (Fig. 2f). Therefore, the **NIR-TS** probe could track the behavior of low-content SO_2 (and its derivatives) in cells.

We wished to investigate the effect and levels of SO_2 during oxidative stress in mitochondria.[16] HeLa cells were treated with LPS, and NIR fluorescent signals documented. However, when LPS-pretreated cells were incubated with 200 μM *N*-acetylcysteine (NAC; antioxidant) and imaged by the **NIR-TS** probe, NIR fluorescent signals were decreased obviously (Fig. 3). These results illustrated that SO_2 could have an anti-oxidative-stress effect in mitochondria, and that its levels increased during oxidative stress.

The concentrations used in the experiments mentioned above for $Na_2S_2O_3$ (500 μM) or LPS (1 μg mL^{-1}) were based on the literature.[17] A certain amount of sulfite could enter cells in a short time and "lighten" the cells, so Na_2SO_3 (50 μM) was selected.

Furthermore, we investigated the capability of the **NIR-TS** probe for imaging SO_2 (and its derivatives) in a mouse model (Fig. 4). For mice injected with the **NIR-TS** probe alone, no NIR fluorescence signals emerged. NIR fluorescence signals appeared for **NIR-TS** probe-pretreated mice injected *in situ* with Na_2SO_3 (50 μM), $Na_2S_2O_3$ (500 μM) or LPS (1 μg mL^{-1}) (Fig. 4b, c and e). However, for control mice pretreated with NEM or FA, the fluorescence signals were reduced significantly (Fig. 4d and f). The results in mice models were consistent with those in cell experiments.

The SO_2 level was increased for LPS-treated mice. However, after mice had been treated with the antioxidant NAC, the SO_2 level decreased (Fig. S10, ESI†). Results showed that SO_2 had an anti-oxidative-stress effect in mice.

Results also showed that the **NIR-TS** probe provided a reliable approach for non-invasive visualization of SO_2 (and its derivatives) in a mouse model during oxidative stress.

In summary, we developed an NIR fluorescent probe which displayed excellent mitochondrial-targeting ability and which could be applied to SO_2 visualization during oxidative stress in HeLa cells as well as in a mouse model. The strategy for constructing the **NIR-TS** probe was different to the traditional

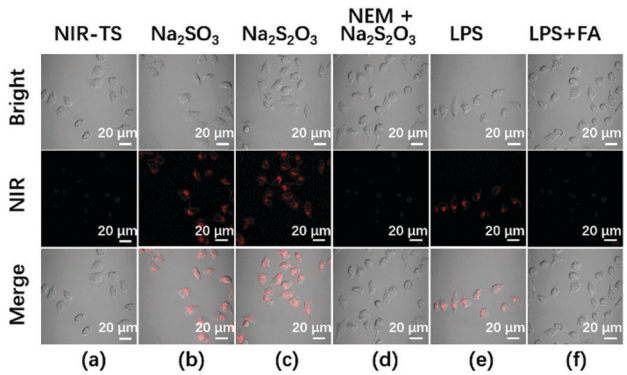

Fig. 2 NIR fluorescence imaging of SO_2 (Na_2SO_3) in HeLa cells. (a) HeLa cells were incubated with the **NIR-TS** probe (10 μM) for 15 min. (b) HeLa cells were pre-treated with the **NIR-TS** probe and then incubated with exogenous Na_2SO_3 (50 μM) for 10 min. (c) HeLa cells were pretreated with the **NIR-TS** probe (10 μM), then incubated with $Na_2S_2O_3$ (500 μM) for 30 min. (d) The **NIR-TS** probe-stained HeLa cells were incubated with 500 μM NEM for 30 min, followed by $Na_2S_2O_3$ for another 30 min. (e) HeLa cells were treated with the **NIR-TS** probe, then incubated with 1 μg mL^{-1} lipopolysaccharide. (f) HeLa cells were incubated with the **NIR-TS** probe, then FA (200 μM) and lipopolysaccharide (1 μg mL^{-1}) were added. Scale bar: 20 μm.

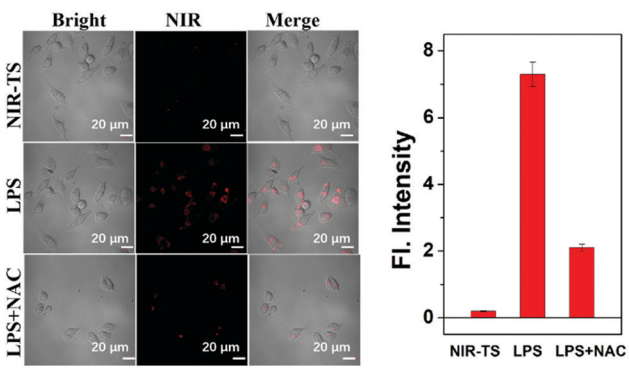

Fig. 3 NIR fluorescence images of HeLa cells. Cells were treated with the **NIR-TS** probe (10 μM); cells were treated with the **NIR-TS** probe (10 μM) and LPS; cells were treated with the **NIR-TS** probe, LPS and NAC (200 μM).

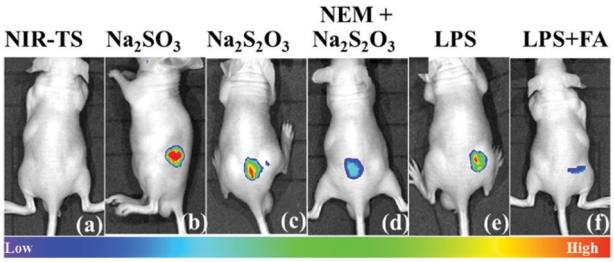

Fig. 4 NIR fluorescence imaging of Na_2SO_3 in mice. (a) **NIR-TS** probe (10 μM)-treated mice. (b), (c) and (e) **NIR-TS** ptobe (10 μM)-treated mice were also injected with Na_2SO_3 (50 μM), $Na_2S_2O_3$ and LPS, respectively. (d) As a control of (c), mice were treated with NEM, then $Na_2S_2O_3$ and the **NIR-TS** probe. (f) As a control of (e), mice were treated with LPS, then FA and the **NIR-TS** probe.

design for NIR fluorophores. Also, we reassessed the unique merits of ESIPT mechanism in designing this **NIR-TS** probe.

This work was supported by the Natural Science Foundation of China (21775096, 21878180), One Hundred People Plan of Shanxi Province, Shanxi Province "1331 project" Key Innovation Team Construction Plan Cultivation Team (2018-CT-1), 2018 Xiangyuan County Solid Waste Comprehensive Utilization Science and Technology Project (2018XYSDJS-05), Shanxi Province Foundation for Returnees (2017-026), Shanxi Collaborative Innovation Center of High Value-added Utilization of Coal-related Wastes (2015-10-B3), Shanxi Province 2019 Annual Science and Technology Activities for Overseas Students Selected Funding Projects, Innovative Talents of Higher Education Institutions of Shanxi, Scientific and Technological Innovation Programs of Higher Education Institutions in Shanxi (2020L0541), Key R&D Program of Shanxi Province (201903D421069), Key R&D and Transformation Plan of Qinghai Province (2020-GX-101) and Scientific Instrument Center of Shanxi University (201512).

Conflicts of interest

None.

Notes and references

1 N. Sang, Y. Yun, H. Li, L. Hou, M. Han and G. K. Li, *Toxicol. Sci.*, 2010, **114**, 226–236.
2 Y. Sun, J. Liu, J. Zhang, T. Yang and W. Guo, *Chem. Commun.*, 2013, **49**, 2637–2639.
3 W. Chen, Q. Fang, D. Yang, H. Zhang, X. Song and J. Foley, *Anal. Chem.*, 2015, **87**, 609–616.
4 (*a*) Z. Meng, *Inhalation Toxicol.*, 2003, **15**, 181–195; (*b*) A. Kubo, H. Saji, K. Tanaka and N. Kondo, *Plant Mol. Biol.*, 1995, **29**, 479–489.
5 (*a*) R. Weissleder and M. J. Pittet, *Nature*, 2008, **452**, 580–589; (*b*) A. Razgulin, N. Ma and J. Rao, *Chem. Soc. Rev.*, 2011, **40**, 4186–4216; (*c*) L. You, D. Zha and E. V. Anslyn, *Chem. Rev.*, 2015, **115**, 7840–7892; (*d*) Y. Wen, F. Huo and C. Yin, *Chin. Chem. Lett.*, 2019, **30**, 1834–1842.
6 (*a*) X. Yang, Y. Zhou, X. Zhang, S. Yang, Y. Chen, J. Guo and X. Li, *Chem. Commun.*, 2016, **52**, 10289–10292; (*b*) X. Yang, W. Liu, J. Tang, P. Li, H. Weng, Y. Ye and M. Xian, *Chem. Commun.*, 2018, **54**, 11387–11390; (*c*) D. Li, Z. Wang, X. Cao, J. Cui, X. Wang, H. Z. Cui, J. Miao and B. X. Zhao, *Chem. Commun.*, 2016, **52**, 2760–2763.
7 W. Zhang, F. Huo, Y. Zhang and C. Yin, *J. Mater. Chem. B*, 2019, **7**, 1945–1950.
8 (*a*) M. Cui, M. Ono, H. Watanabe, H. Kimura, B. Liu and H. Saji, *J. Am. Chem. Soc.*, 2014, **136**, 3388–3394; (*b*) X. Wang, Z. Guo, S. Zhu, H. Tian and W. H. Zhu, *Chem. Commun.*, 2014, **50**, 13525–13528; (*c*) W. Chen, S. Xu, J. J. Day, D. Wang and M. Xian, *Angew. Chem.*, 2017, **129**, 16838–16842; (*d*) V. R. Mishra, C. W. Ghanavatkar and N. Sekar, *ChemistrySelect*, 2020, **5**, 2103–2113.
9 V. R. Mishra, C. W. Ghanavatkar and N. Sekar, *ChemistrySelect*, 2020, **5**, 2103–2113.
10 (*a*) H. Wen, Q. Huang, X. F. Yang and H. Li, *Chem. Commun.*, 2013, **49**, 4956–4958; (*b*) X. F. Yang, Q. Huang, Y. Zhong, Z. Li, H. Li, M. Lowry, J. O. Escobedo and R. M. Strongin, *Chem. Sci.*, 2014, **5**, 2177–2183; (*c*) Q. Wang, L. Zhou, L. Qiu, D. Lu, Y. Wu and X. B. Zhang, *Analyst*, 2015, **140**, 5563–5569; (*d*) V. S. Patil, V. S. Padalkar, A. B. Tathe and N. Sekar, *Dyes Pigm.*, 2013, **98**, 507–517.
11 (*a*) Y. Liu, K. Li, K. Xie, L. Li, K. Yu, X. Wang and X. Q. Yu, *Chem. Commun.*, 2016, **52**, 3430–3433; (*b*) E. Karakuş, M. Üçüncü and M. Emrullahoğlu, *Anal. Chem.*, 2016, **88**, 1039–1043.
12 (*a*) Y. Liu, K. Li, K. X. Xie, L. L. Li, K. K. Yu, X. Wang and X. Q. Yu, *Chem. Commun.*, 2016, **52**, 3430–3433; (*b*) A. J. Ji, S. R. Savon and D. W. Jacobsen, *Clin. Chem.*, 1995, **41**, 897–903.
13 Y. Ma, Y. Tang, Y. Zhao, S. Gao and W. Lin, *Anal. Chem.*, 2017, **89**, 9388–9393.
14 H. Mitsuhashi, S. Yamashita, H. Ikeuchi and T. Kuroiwa, *Shock*, 2005, **24**, 529–534.
15 J. J. Zhang, Y. X. Fu, H. H. Han, Y. Zang, J. Li, X. P. He, B. L. Feringa and H. Tian, *Nat. Commun.*, 2017, **8**, 987–996.
16 J. Z. Li, Y. H. Sun, C. Y. Wang, Z. Q. Guo, Y. J. Shen and W. H. Zhu, *Anal. Chem.*, 2019, **91**, 11946–11951.
17 W. Chen, Q. Fang, D. Yang, H. Zhang, X. Song and J. Foley, *Anal. Chem.*, 2016, **88**, 4426–4431.